

pubs.acs.org/JACS Article

Oxidative Stability Matters: A Case Study of Palladium Hydride Nanosheets for Alkaline Fuel Cells

Huiqi Li,[§] Rui Zeng,[§] Xinran Feng,[§] Hongsen Wang, Weixuan Xu, Xinyao Lu, Zhaoxiong Xie,* and Héctor D. Abruña*



Cite This: J. Am. Chem. Soc. 2022, 144, 8106-8114



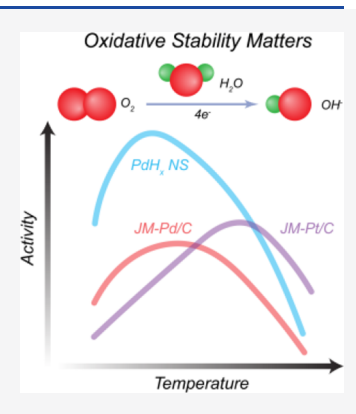
ACCESS I

Metrics & More

Article Recommendations

SI Supporting Information

ABSTRACT: Pd-based electrocatalysts are considered to be a promising alternative to Pt in anion-exchange membrane fuel cells (AEMFCs), although major challenges remain. Most of the Pd-based electrocatalysts developed for the sluggish oxygen reduction reaction (ORR) have been exclusively evaluated by rotating disk electrode (RDE) voltammetry at room temperature, rather than in membrane electrode assemblies (MEAs), making it challenging to apply them in practical fuel cells. We have developed a series of carbon-supported novel PdH_x nanosheets (PdH_x NS), which displayed outstanding ORR performance in room-temperature RDE tests. Specifically, a sample synthesized at 190 °C displayed a mass activity of 0.67 A mg⁻¹ and a specific activity of 1.07 mA cm⁻² at 0.95 V vs RHE, representing the highest reported value among Pd-based ORR electrocatalysts in alkaline media and higher than Pt-based catalysts reported in the literature. Furthermore, we employed PdH_x NS and commercial Pd/C as model catalysts to systematically study the effects of temperature on their ORR activity in RDE measurements and subsequently evaluated their performance in MEA testing. Our observations indicate/demonstrate how oxidative stability affected the ORR performance of Pd-based electrocatalysts, which provided some critical insights into future ORR catalyst development for alkaline fuel cell applications.



INTRODUCTION

Anion-exchange membrane fuel cells (AEMFCs) have made significant advances in recent times and now display great potential to become an alternative to proton exchange membrane (PEM) fuel cells. The sluggish ORR kinetics in fuel cells, however, requires the use of large amounts of Pt. Hence, there is a pressing need to develop and explore other non-Pt based and non-noble metal electrocatalysts to alleviate our reliance on Pt. Previous studies have shown that the ORR activity of Pd is comparable to that of Pt among noble metalbased single crystals in alkaline media, indicating that Pd can be a promising alkaline ORR electrocatalyst. Recently, there have been reports of improved ORR performance with Pdbased electrocatalysts in alkaline media, which even outperformed Pt-based electrocatalys.³⁻⁹ Among those highperformance Pd-based electrocatalysts, Pd-based nanosheets exhibited some of the highest ORR activities, as their twodimensional (2D) structure provided a high specific surface area, strain effects with atomic thickness, as well as high density of unsaturated atoms exposed on the surface. 9,10 Moreover, Pd hydride (PdH_r) has been demonstrated to play an important role in enhancing ORR activity. 11,12

Although dramatic improvements in ORR activity in alkaline media have been achieved with Pd-based electrocatalysts, there have been very limited reports on Pd-based systems that exhibit higher performance than that of Pt in AEMFC testing based on membrane electrode assemblies (MEAs). The

majority of reported Pd-based electrocatalysts have been exclusively studied in the liquid electrolyte using a rotating disk electrode (RDE), but rarely in an MEA. The RDE testing method is a well-established procedure that has been widely accepted for determining the mass activity and specific activity of catalysts, playing a key role in the preliminary screening of high-performance electrocatalysts. Nevertheless, a high activity under RDE conditions does not necessarily guarantee the same performance in an MEA because their ORR operating conditions are substantially different. 13,14 For instance, most RDE measurements are conducted at room temperature in liquid electrolyte with low O2 solubility, while MEA experiments are carried out at much higher temperatures (60-80 °C) using an ion-exchange polymer electrolyte. 15 For Pd-based electrocatalysts, the oxidative stability is supposed to play a dominant role in determining the ORR performance, given that Pd is more easily oxidized by oxygen than Pt-based electrocatalysts, especially under the MEA's harsh testing conditions. Unfortunately, the oxidative stability has been

Received: January 14, 2022 Published: April 29, 2022





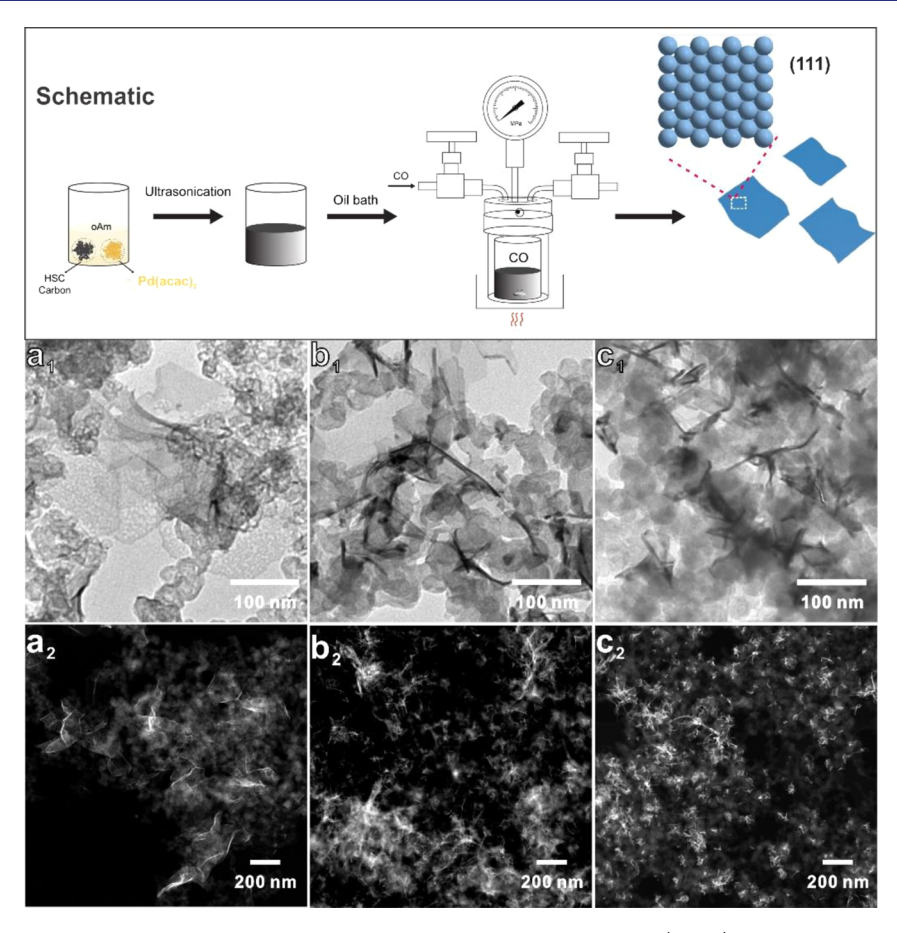


Figure 1. Schematic of synthesis procedure and morphology of carbon-supported PdH_x NS. (a_1-c_1) TEM images and (a_2-c_2) corresponding STEM images of carbon-supported PdH_x NS-80, PdH_x NS-140, and PdH_x NS-190.

rarely recognized and systematically studied in regular RDE tests.

In this study, we focus on the oxidative stability of Pd-based electrocatalysts. First, we successfully synthesized a series of PdH_x nanosheets supported on high-surface-area carbon (PdH_x NS) by controlling the synthesis temperature and CO pressure. We then rigorously evaluated the ORR performance of the as-synthesized PdH, NS in alkaline media and compared their performance to that of commercial Pd/C and Pt/C. Our results indicate that these PdH_x NS exhibit outstanding ORR activity. In particular, a sample synthesized at 190 °C (PdH_x NS-190) displayed a mass activity of 0.67 A mg⁻¹ and a specific activity of 1.07 mA cm⁻² at 0.95 V vs RHE, representing the highest reported value for Pd-based ORR electrocatalysts in the literature. We next explored how the oxidative stability of Pd-based electrocatalysts affected their ORR performance in alkaline media by employing PdH, NS and commercial Pd/C as model catalysts. Finally, we demonstrate that the excellent ORR performance of PdH_r NS displayed at room temperature could not be sustained at high temperatures, mainly due to low oxidative stability. This finding was also confirmed by realistic fuel cell evaluations based on MEAs and stressed the importance of oxidative stability of ORR electrocatalysts for practical fuel cell applications.

■ RESULTS AND DISCUSSION

Synthesis and Structural Characterization of Carbon-Supported PdH, Nanosheets. Carbon-supported PdH, NSs were synthesized via a one-pot solvothermal method, as illustrated in the synthesis schematic (Figure 1). Pd(acac)₂ was employed as the precursor while CO acted both as the reductant and a morphological regulator. The synthesis details can be found in the Supporting Information. By controlling the synthesis temperature (80, 140, and 190 °C) and CO pressure, a series of highly dispersed carbon-supported PdH, NSs was obtained (denoted as PdH_x NS-80, PdH_x NS-140, and PdH_x NS-190, respectively). The morphology of the as-synthesized carbon-supported PdH, NSs was first investigated via transmission electron microscopy (TEM) and scanning transmission electron microscopy (STEM) (Figure 1a₁-c₁, Figure $1a_2-c_2$). The as-prepared PdH_x NSs were homogeneously distributed over the carbon support, which promoted the dispersion of the nanosheets during the growth process. The PdH_x NS-80 sample displayed ultrathin PdH_x nanosheets with lateral sizes reaching more than 200 nm, making them very susceptible to electron beam damage during characterization. 16 With increasing synthesis temperature, the nanosheets tended to fold and curl at the edges, yielding a relative increase in thickness but a shrinkage in size.

The crystal structures and phases of the PdH_x NSs were analyzed with X-ray diffraction (XRD). As shown in Figure 2a, the XRD patterns of PdH_x NSs synthesized at different temperatures displayed the same characteristic spectral patterns, typical of the face-centered cubic (fcc) structure. Compared to the Pd standard reference, however, the PdH_x NSs exhibited clear shifts to lower 2θ values, indicating an increase in the lattice parameter. The lattice expansion is

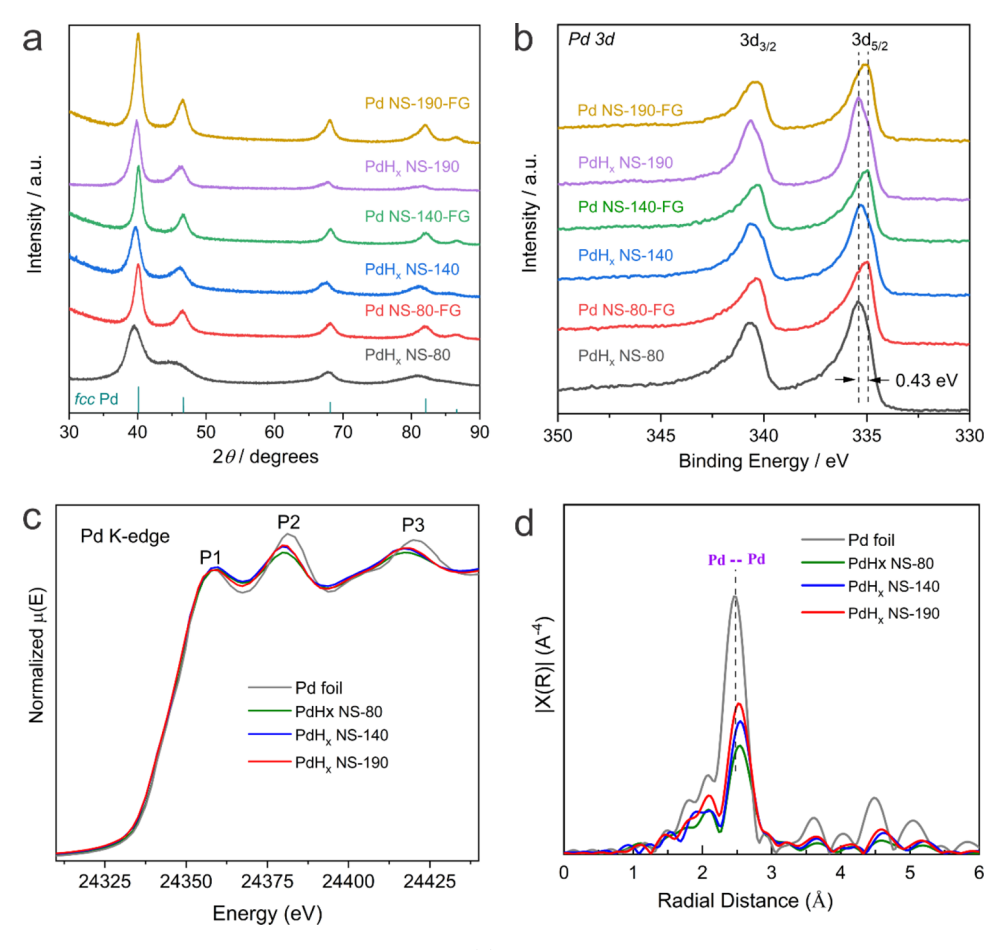


Figure 2. X-ray characterization of the structure of Pd-based NS. (a) XRD patterns of PdH_x NS electrocatalysts, and comparison to fcc Pd reference. (b) XPS high-resolution spectra of Pd 3d orbitals $(3d_{3/2} \text{ and } 3d_{5/2})$. (c) XANES spectra and (d) Fourier transform (FT) of k^3 -weighted EXAFS spectra of PdH_x NS synthesized at different temperatures. A reference Pd foil is also shown for comparison.

unlikely to be due to alloying with metals with larger radii because no other metal was employed in the synthesis. Consequently, the significant increase in the lattice parameter likely resulted from hydrogen incorporation, as Pd is known to incorporate hydrogen atoms into the interstitial sites, leading to a lattice expansion. The hydride formation was further corroborated by annealing the treated samples, which subsequently exhibited the XRD patterns that matched well with the Pd standard reference. This observation represents compelling evidence that the annealing treatment promoted the release of hydrogen in the Pd lattice, confirming the presence of palladium hydride. X-ray photoelectron spectroscopy (XPS) was also used to probe the chemical states of Pd in PdH_x NSs. Figure 2b presents high-resolution spectra of Pd 3d orbitals, in which the characteristic spin-orbit splitting leads to 3d_{3/2} and 3d_{5/2} peaks with an energy spacing of 5.3 eV. Compared to their corresponding annealed counterparts, PdH_x NSs exhibited a shift toward a higher binding energy of 0.43 eV, suggesting that electron transfer from Pd to H leads to a downshift of the d-band center.¹⁹

Synchrotron-based X-ray absorption spectroscopy (XAS) was employed to further characterize the geometric structure, coordination environment, and electronic states of Pd in PdH $_x$ NSs. The X-ray absorption near edge structure (XANES) spectra of the Pd K-edge were acquired and calibrated against a Pd foil with an edge energy of 24,350 eV. As presented in Figure 2c, the relatively smaller energy difference between the

P1 and P2 peaks of PdH, NSs samples, relative to the Pd foil, indicates that the d-band center shifted to lower energy, in good agreement with XPS observations. 19,20 In addition to the information from the XANES spectra, the extended X-ray absorption fine structure (EXAFS) spectra provided more detailed insights into the coordination environment of Pd and Pd-Pd bond distances. Figure 2d shows the k^3 -weighted EXAFS spectra after Fourier transforming, in which the strongest peak at around 2.5 Å corresponds to the first scattering shell of Pd-Pd. In contrast to Pd foil, three kinds of PdH_x NSs displayed clearly longer radial distances for the first scattering shell, suggesting that H incorporation led to a lattice expansion, consistent with the XRD results. Additionally, the intensities in the Fourier transform (FT) of PdH_x NSs were significantly reduced, likely resulting from the much lower overall coordination numbers relative to bulk Pd. Furthermore, the incorporation of hydrogen atoms into the lattice could give rise to structural disordering to some extent and further reduce the intensities of FT peaks. ¹⁹ It is also worth noting that PdH_x NSs synthesized at different temperatures displayed slightly different oscillation intensities, suggesting non-negligible changes in their coordination environment. Specifically, the intensities increased in following sequence: PdH_x NS-80 < PdH_x NS-140 < PdH_x NS-190, suggesting increased coordination numbers with increasing temperature. This feature likely originated from the curling and thickening of the nanosheets, as observed in the TEM and STEM images.

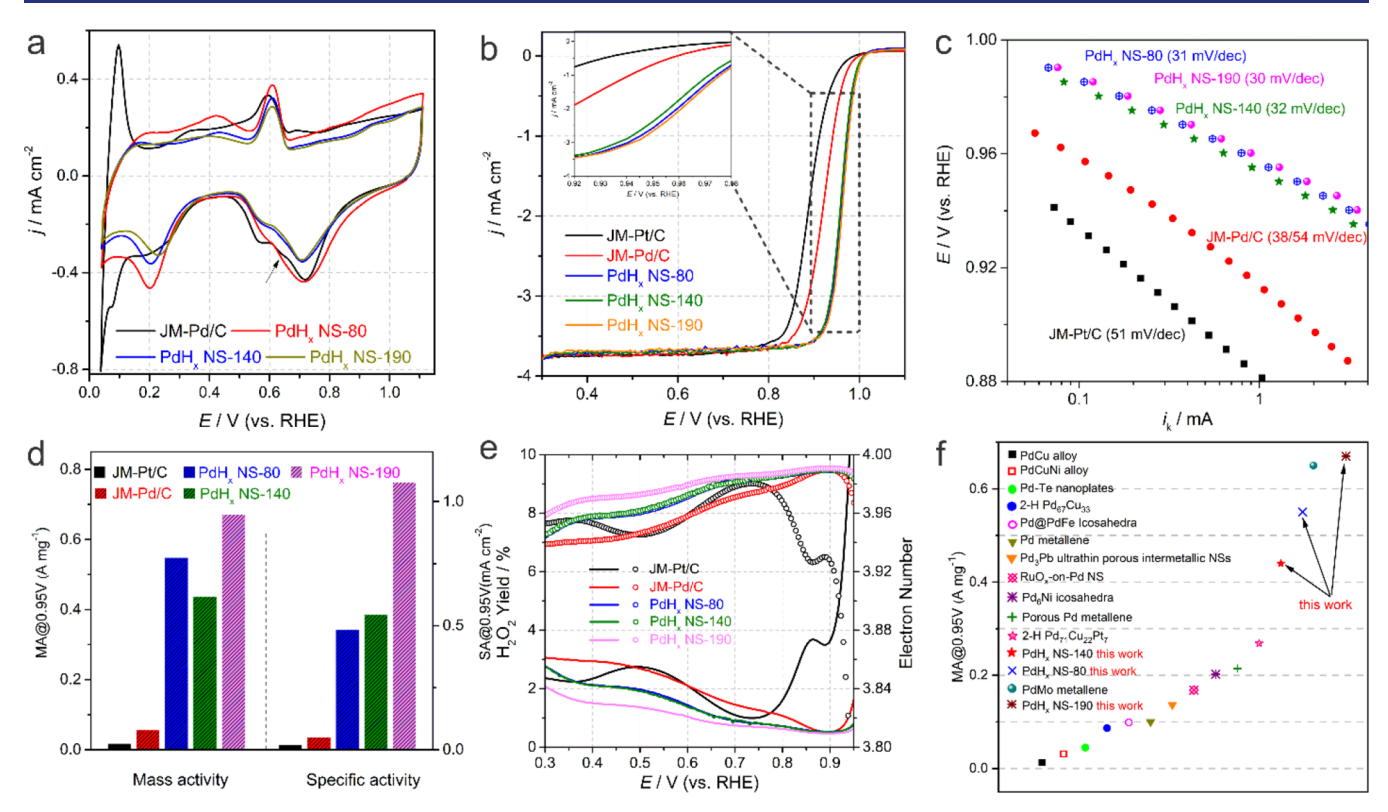


Figure 3. Electrochemical properties of PdH_x NS compared to commercial Pt/C and Pd/C. (a) CV in Ar-saturated 1 M KOH solution (scan rate: 20 mV/s); arrow is intended to indicate the presence of shoulder peaks in the voltametric profiles for PdH_x NS-80 and JM-Pd/C, respectively; (b) anodic scan of ORR polarization curves in O_2 -saturated 1 M KOH solution (scan rate: 5 mV/s; rotation rate: 1600 rpm). The current was normalized to the geometric area of the electrode. The inset shows the magnified kinetic-diffusion controlled regions for better comparison; (c) ORR Tafel plot with kinetic current extracted from (b); (d) mass activity (MA) and specific activity (SA) obtained via normalizing the kinetic current extracted at 0.95 V vs RHE; (e) ORR selectivity measured by RRDE; (f) ORR activity comparison among the literature-reported Pd-based electrocatalysts measured at 0.95 V vs RHE (detailed information is available in Table S2).

Electrocatalytic Evaluation of Carbon-Supported PdH_x Nanosheets. The electrochemical properties of carbon-supported PdH_r NSs were evaluated in 1 M KOH with RDE voltammetry. Figure 3a presents the cyclic voltammograms (CV) of carbon-supported PdH_x NSs and commercial JM-Pd/C, which enabled the identification of surface structural features. Different from Pt/C (Figure S1a), the Pd-based catalysts displayed asymmetric hydrogen adsorption/desorption features without a well-defined double layer, probably due to hydrogen absorption and complex OH adsorption process.²¹ While Pd/C exhibited strong characteristic hydrogen absorption features below 0.2 V vs RHE, similar patterns in the carbon-supported PdH, NSs catalysts were significantly suppressed. This sharp contrast is reasonable because there would be few available spaces for further hydrogen absorption once the Pd lattice is filled with stable hydrogen atoms after palladium hydride formation. In the anodic scan, a symmetric peak emerged at 0.6 V, likely due to the oxidation of Pd{111} facets.²¹ At higher potentials, the oxidation current gradually increased but without prominent oxidation peaks, eliminating contributions from $Pd\{100\}$ facets. ^{22,23} In the cathodic scans, a significant peak, assigned to the reduction of oxidized Pd, could be observed near 0.7 V. It is worth noting that both Pd/C and PdHx NSs catalysts displayed a clear shoulder near 0.57 V, in agreement with the previously reported CV features of Pd{111} single crystals.²² This observation suggests that the surfaces of PdH_x NSs and Pd/C catalysts are dominated by Pd{111} facets. Moreover,

Pd/C exhibited an additional shoulder at 0.64 V, which could be ascribed to Pd{111} or Pd{100} steplike sites on the surface. These steplike features, however, were relatively weaker in the PdH $_x$ NS-80 and PdH $_x$ NS-140 catalysts and even absent in PdH $_x$ NS-190. These results revealed that the step site density in PdH $_x$ NSs catalysts is significantly lower than that on Pd/C and decreases with increased synthesis temperature, consistent with the increase in the average coordination numbers, as inferred from the EXAFS spectra. These observations highlight the importance of employing CV features for surface structure identification.

The ORR performance was tested in an O2-saturated 1 M KOH solution at a rotation rate of 1600 rpm. Figure 3b presents the ORR polarization profiles of the carbon-supported PdH, NSs, compared to the benchmark catalysts of commercial Pt/C and Pd/C. In the lower potential regions (0.3-0.8 V), those catalysts displayed a well-defined diffusionlimited current density, converging at 3.75 mA/cm², a value indicative of a four-electron process. It should be noted that this value is lower than that commonly reported in 0.1 M KOH solution (ca. 5.7 mA/cm²) because the O₂ solubility in 1 M KOH solution decreases to ~70% of that in 0.1 M KOH solution.²⁵ In the kinetic and mass-transport-controlled regions, those catalysts exhibited significantly different electrocatalytic properties. All three carbon-supported PdH_x NS catalysts displayed superior ORR performance, with half-wave potentials $(E_{1/2})$ positive to those of Pt/C and Pd/C, by more than 70 and 40 mV, respectively. The much smaller Tafel slope

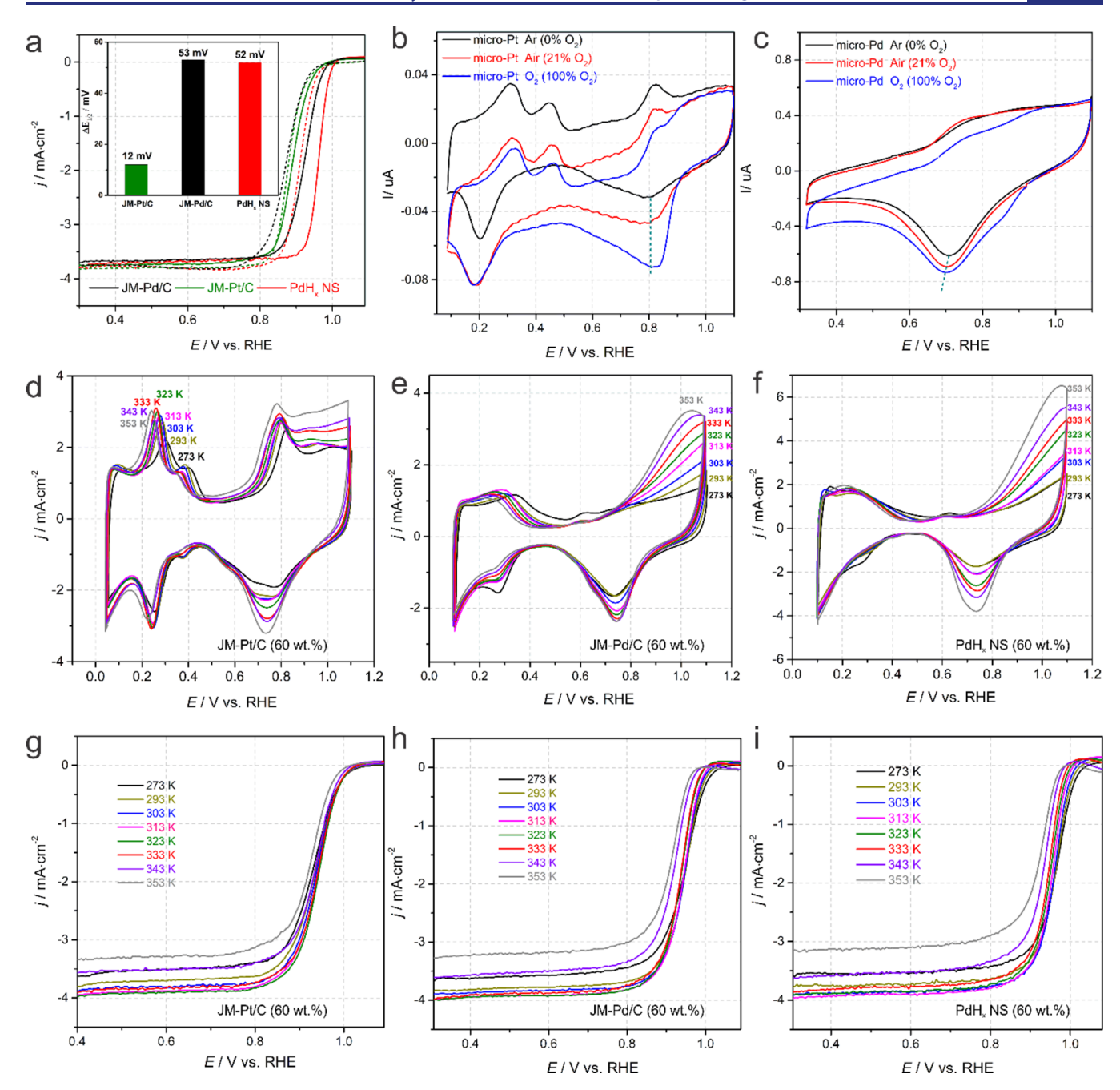


Figure 4. Oxidative stability evaluation of PdH_x NS catalysts. (a) ORR polarization curves of 20 wt % commercial Pt/C, Pd/C, and PdH_x NS with anodic (solid) and cathodic (dashed) scans; inset displays half-wave potential differences between the two scans; (b,c) CV curves of Pt and Pd microelectrodes in argon- $(0\% O_2)$, air- $(21\% O_2)$, and oxygen-saturated $(100\% O_2)$ 1 M KOH solution at a scan rate of 2000 mV/s; (d-f) CV profiles of 60 wt % commercial Pt/C (d), Pd/C (e), and PdH_x NS (f) measured between 273 and 353 K in Ar-saturated 1 M KOH solution (scan rate: Pt/C (g), Pt/C (h), and Pt/C (h), and Pt/C (i) measured between 273 and 353 K in O_2 -saturated 1 M KOH solution (scan rate: Pt/C (g), Pt/C (h), and Pt/C (h), and Pt/C (g) measured between 273 and 353 K in O_2 -saturated 1 M KOH solution (scan rate: Pt/C (g), Pt/C (h), and Pt/C (h), and Pt/C (g) measured between 273 and 353 K in O_2 -saturated 1 M KOH solution (scan rate: Pt/C (g), Pt/C (h), and Pt/C (h), and Pt/C (g), Pt/C (h), and Pt

(TS) shown in Figure 3c further confirmed the enhanced reaction kinetics of the carbon-supported PdH_x NS catalysts. It should be noted that the lattice H remained stable after ORR tests (Figure S2). In order to further quantify the ORR activities, the kinetic currents derived from the Koutecký–Levich equation, at 0.95 V, were normalized to the mass and electrochemical surface areas (ECSAs) (Figures S1b–d and Table S1), respectively, yielding mass activity (MA) and specific activity (SA). As shown in Figure 3d, carbon-supported PdH $_x$ NS catalysts significantly outperformed commercial Pt/C and Pd/C by more than 30 and 10 times,

respectively, with PdH_x NS-190 exhibiting the highest MA at 0.67 A/mg. Moreover, the SA of PdH_x NS-190 approached 1.1 mA/cm², corresponding to 60- and 21-fold enhancements over Pt/C and Pd/C, respectively. When compared with the literature, PdH_x NS-190 represents the most active one among reported Pd-based ORR catalysts (Figure 3f and Table S2). We ascribe this impressive activity to not only its superior intrinsic activity but also to good dispersion, resulting from the carbon support, which mitigated agglomeration and aggregation of nanosheets during synthesis (Figure S3).

It is worth noting that the intrinsic activities of PdH_x NSs catalysts exhibited a dependence on synthesis temperature with the following order: PdH_x NS-80 < PdH_x NS 140 < PdH_x NS-190, which is opposite to contributions from step sites. This correlation suggests that the ORR activity is closely associated with changes in the active sites on the surface, which would be an anticipated result. Specifically, Pd{111} has been reported to exhibit the highest ORR performance in alkaline media compared to the other two low index facets, and the presence of step sites could result in lower ORR activity.²² Because the surface of PdH_x NS-190 was dominated by {111} facets with minimal step sites, it is reasonable that PdH_x NS-190 exhibited the highest activity among the three PdH_x NS catalysts studied here. However, the small difference in voltametric features, arising from step sites in Figure 3a, may not be enough to account for the almost twofold difference in activity between PdH_x NS-190 and NS-140, as shown in Figure 3d. It is likely that the increase in nanosheet thickness also contributes to the observed ORR performance, as indicated by the narrower diffraction peaks (Figure 2a) and smaller ECSAs (Figure S1d and Table S1) with increased synthesis temperature. Pd and Pt nanoparticles are known to exhibit strong particle size effects; the SA could increase by more than a factor of 2 when the average particle size changed from 3 to 5 nm.²⁶ Accordingly, the thicker nanosheets in PdH_x NS-190 likely played a role in boosting its SA. Moreover, the H/Pd ratios, estimated from 2θ values in the XRD patterns (Figure 2a), differ by 5% for PdH_x NS-140 (17%) and NS-190 (12%), which may further contribute to the improved ORR performance.

To evaluate the long-term stability of the most active PdH_x NS catalysts, accelerated durability testing was conducted in O_2 -saturated 1 M KOH over the potential region from 0.6 to 0.95 V at a scan rate of 100 mV/s for 10,000 cycles. The catalyst displayed a clear diminution of the surface area (Figure S4) and the morphology of the original nanosheets became porous, likely due to electrochemical dissolution and oxidation of Pd as well as detachment of some nanosheets from the substrate. Moreover, the ORR polarization curve exhibited a negative shift of 20 mV compared to the initial one. Nevertheless, the half-wave potential was still much higher than those of commercial Pd/C and Pt/C electrocatalysts.

The ORR selectivity (H_2O or H_2O_2) of the catalysts was assessed by the rotating ring disk electrode (RRDE) voltammetry, in which the potential of the Pt ring was held at 1.3 V to capture any H₂O₂ generated at the disk. Figure 3e presents the calculated H₂O₂ yield and the electron transfer number at different potentials, derived from the measured ring and disk currents. Generally, all the Pd catalysts exhibited an increase in the H₂O₂ yield when moving from higher potentials to lower ones, with a clear decline in the electron transfer number. This is likely due, at least in part, to the increased ORR current generated from the carbon support, which cannot completely reduce O₂ to H₂O but, instead, produces H₂O₂.²⁷ Overall, the PdH_x NSs catalysts exhibited significantly lower H₂O₂ yields and higher electron transfer numbers when compared to Pt/C and Pd/C, indicating excellent selectivity for the four-electron reduction of O_2 to H_2O . Among them, PdH_r NS-190 displayed the lowest H_2O_2 yield (<2%) over the studied potential range, with peroxide yields as low as 0.44% at 0.9 V and an average electron transfer number of 3.96, very close (and within experimental error) to the 4-electron process. These RRDE results indicate that PdH_x NSs catalysts can effectively promote the complete reduction of oxygen,

contributing to an improved energy efficiency and operational stability in fuel cells.

The Effects of Oxidative Stability on the ORR **Performance.** While PdH_x NS catalysts displayed remarkable ORR activity in aqueous media, it remained unclear whether PdH_x NS catalysts could withstand oxidation, especially under the oxygen-rich and high-temperature conditions of real fuel cell tests. Unfortunately, the oxidation stability performance of Pd-based catalysts has been largely neglected in the literature. Consequently, it was of great importance and interest to investigate the oxidative stability of PdH_x NS catalysts. Figure 4a presents the ORR polarization profiles, including both anodic and cathodic scans, for 20 wt % catalysts. Compared to Pt/C, both Pd/C and PdH_x NS displayed significant hysteresis, with the cathodic scan being much more negative than the anodic scan. Specifically, the half-potential difference ($\Delta E_{1/2}$) between two scans increased from 12 mV for Pt/C to 53 mV and 52 mV for Pd/C and PdHx NS, respectively, suggesting that the surfaces of Pd-based catalysts are easier to oxidize when compared to Pt. A similar trend was also found with 60 wt % catalysts, usually used in MEA tests (Figure S5). To further evaluate the importance of oxidative stability, it is critical to examine the effects of oxygen concentration and temperature on the ORR performance because the typical oxidation processes are governed by the concentration of O2 and temperature.

Pd and Pt microelectrodes were employed to study the effects of oxygen concentration because the iR drop could be significantly reduced compared to regular RDE electrodes at high scan rates and the mass transport could be effectively improved with an electrode size that is comparable to the thickness of the diffusion layer. Figure 4b,c shows the ORR polarization profiles of Pt and Pd microelectrodes at a scan rate of 2000 mV/s, with the O₂ content increasing from 0 to 21 and 100%. The high scan rate helped the reduction peak of the oxidized surface stand out from the ORR background current, which provided insights into the surface oxidation reduction features. In contrast to the Pt microelectrode, in which the reduction peak potential barely changed (Figure 4b), the Pd microelectrode displayed a clear and significant negative shift in the reduction peak potential with increasing oxygen content (Figure 4c), indicating that Pd is more likely to be influenced by the O_2 concentration.

The temperature-dependent ORR kinetics were investigated over the temperature range from 0 °C (273 K) to 80 °C (353 K). As presented in Figure 4d-f, the CV indicated that all the catalysts experienced increased oxidation currents, as a result of increased coverage of OH and oxide species, at higher potentials with increasing temperatures. The oxidation patterns of Pd/C and PdH_x NS became much more prominent than those of Pt/C, especially at potentials beyond 0.9 V. In particular, the oxidation current of Pd/C and PdH_x NS at 0.9 V increased by over a factor of 2 while less than an 80% increase was observed for Pt/C. This finding again suggested that increasing the temperature could lead to accelerated surface oxidation. Figure 4g-i shows the ORR polarization curves for Pt/C, Pd/C, and PdHx NS measured at different temperatures. Of particular note are the significant changes in the diffusion-limited current densities with temperature, primarily as a result of temperature-dependent variations in oxygen solubility, diffusion coefficients, and kinematic viscosity.

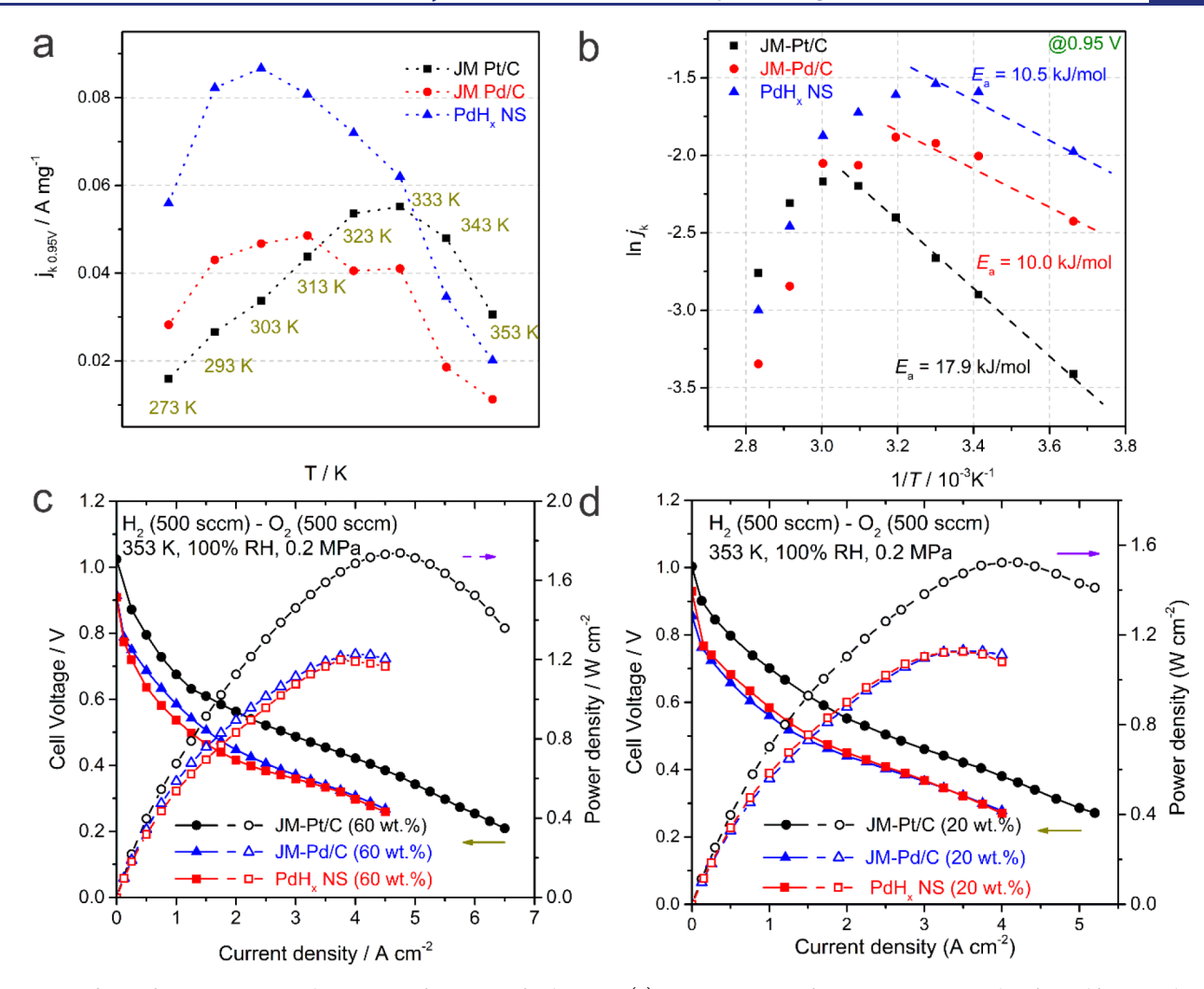


Figure 5. Effects of temperature on the ORR performance of PdH_x NS. (a) Mass activities of 60 wt % commercial Pt/C, Pd/C, or PdH_x NS determined at 0.95 V in anodic scan as a function of temperature. The mass activity was also normalized to the O_2 concentration by referencing to that at 293 K as 1; (b) Arrhenius plots with current density extracted from (a); (c) single cell AEMFC performance with 60 wt % commercial Pt/C, Pd/C, or PdH_x NS as the cathode (0.4 mg_{Pt+Ru}/cm^2) and 60 wt % commercial Pt/C performance with 20 wt % commercial Pt/C, Pd/C, or PdH_x NS as the cathode (0.1 mg_{metal}/cm^2) and 60 wt % commercial Pt/C as the anode (0.4 mg_{Pt+Ru}/cm^2). The cell was fed with 500 sccm H_2 and H_2 and H_3 and tested at 353 K with 100% relative humidity and 0.2 MPa backpressure.

The mass-normalized kinetic current densities were extracted from the ORR polarization curves to quantitatively understand the effects of temperature on the ORR performance across different catalysts (Figures 5a and S6a,b). It is worth noting that the kinetic current densities were also normalized to the O2 concentrations in an effort to eliminate the effects from the temperature-dependent changes in O2 concentrations (Table S3).²⁸ As shown in Figure 5a, the ORR activity of all catalysts measured at 0.95 V displayed a similar volcano-type response with increasing temperature. PdH_x NS and Pd/C reached their maximum at 303 and 313 K, respectively, while the turning point for Pt/C occurred only above 333 K. The most noteworthy aspect of this feature was that the ORR activity of Pt/C surpassed those of PdH_x NS and Pd/C at temperatures above 343 K, even though they exhibited much higher ORR activity than Pt/C at lower temperatures. This observation indicates that the superior ORR performance of PdH_x NS achieved at room temperature could not be maintained under fuel cell operating temperatures. The nonmonotonic profile suggested that temperature could affect the ORR performance from at least two aspects.

On the one hand, the increase in temperature could promote the ORR kinetics via a thermal activation process, which is dominant at lower temperatures. This is further supported by the Arrhenius plots (Figures 5b and S6c,d), which indicated that PdH $_x$ NS and Pd/C displayed weak thermal activation behaviors with apparent activation energies of ~10 kJ/mol at 0.95 V, significantly lower than that of Pt/C (17.9 kJ/mol) (Figure 5b). On the other hand, the increasing temperature could also accelerate surface oxidation of the catalysts, leading to severe degradation in ORR performance at higher temperatures. Thus, it is reasonable to expect that the ORR performance of PdH $_x$ NS and Pd/C could be significantly affected by temperature, given that they displayed poorer oxidative stability.

Both the O₂ concentration and temperature dependence results suggested that the Pd-based catalysts are more likely to be influenced by oxidation, and thus, their ORR performance could be severely impacted in the much harsher fuel cell conditions with high O₂ content and high temperature. PdH_x NS, Pd/C, and Pt/C were employed as cathode catalysts in MEAs to validate their ORR performance under real fuel cell

testing conditions. Figure 5c,d shows the polarization curves of an AEMFCs in H2-O2 mode with PtRu/C as the anode catalyst, illustrating the changes in cell potential and power density as a function of current density. At the beginning, PdH_x NS and Pd/C displayed similar open-circuit potentials of \sim 0.91 V, somewhat lower than that of Pt/C (1.02 V), likely as a result of more oxidized surface. The following rapid voltage drop is likely due to kinetic losses before the curves reached a linear region, where the voltage loss is dominated by Ohmic resistance. Further increases in the current density could yield mass transport losses, in which case a peak in power density (PPD) could be achieved. Thus, the power density displayed a parabolic shape as a response to current density. As illustrated in Figure 5c, Pt/C outperformed both PdH_x NS and Pd/C with a PPD of 1.74 W/cm², a value that is over 40% higher than those of PdH_x NS and Pd/C (1.23 W/cm²). Thus, this observation clearly demonstrates that PdH_x NS and Pd/C are inferior to Pt/C under real fuel cell operating conditions, consistent with the predictions from the temperature-dependent RDE results. A similar trend can also be observed in Figure 5d with a lower catalyst loading (20%), except for a slight decrease in overall performance. Of particular note is that PdH_x NS and Pd/C displayed very similar fuel cell performance in spite of their differences in the structure and morphology, indicating that the oxidized surface played a major role during the fuel cell testing conditions. The possible structural degradation of PdH, NS was ruled out because the XAS results indicated that the hydrogen stably remained in PdH_x NS (Figure S7). Therefore, the poor oxidative stability of Pd-based catalysts might be a road block for their application in fuel cells. Future studies on Pd-based catalysts should be more focused on developing strategies to improve the oxidative stability at elevated temperatures and high O2 concentrations, rather than merely reporting their ORR activity at room temperature. The narrow ORR hysteresis in anodic and cathodic scans and weak temperature-dependent activity degradation might be useful criteria for designing practical future Pd-based ORR catalysts.

CONCLUSIONS

A series of carbon-supported PdH_x nanosheets with high dispersion was successfully prepared and thoroughly examined by TEM/STEM, XRD, XPS, and XAS characterizations. The electrochemical study revealed that the as-synthesized PdH_x NS catalysts possessed dominant Pd{111} facets with a few step site features and thus displayed superior ORR activity and excellent reaction selectivity toward the four-electron reduction of O₂ to H₂O. In particular, PdH_x NS-190 exhibited a recordhigh activity among reported Pd-based ORR catalysts. Nevertheless, the remarkable ORR performance of PdH_x NS observed at room temperature could not be maintained at high temperatures, as a result of poor oxidative stability. This observation was also supported by realistic fuel cell evaluation based on MEAs. Thus, these findings highlight the importance of oxidative stability of ORR catalysts, which is critical for future ORR catalyst development for fuel cell applications.

ASSOCIATED CONTENT

Supporting Information

The Supporting Information is available free of charge at https://pubs.acs.org/doi/10.1021/jacs.2c00518.

Chemicals, synthesis, structural characterization, electrochemical measurements. Supporting figures of the supplementary experimental results including Figures S1-S7 and Tables S1-S3 (PDF)

AUTHOR INFORMATION

Corresponding Authors

Zhaoxiong Xie – State Key Laboratory of Physical Chemistry of Solid Surfaces, Collaborative Innovation Center of Chemistry for Energy Materials, College of Chemistry and Chemical Engineering, Xiamen University, Xiamen, Fujian 361005, China; orcid.org/0000-0002-4225-6536; Email: zxxie@xmu.edu.cn

Héctor D. Abruña - Department of Chemistry and Chemical Biology, Cornell University, Ithaca, New York 14853, United States; orcid.org/0000-0002-3948-356X; Email: hda1@ cornell.edu

Authors

Huiqi Li - Department of Chemistry and Chemical Biology, Cornell University, Ithaca, New York 14853, United States; State Key Laboratory of Physical Chemistry of Solid Surfaces, Collaborative Innovation Center of Chemistry for Energy Materials, College of Chemistry and Chemical Engineering, Xiamen University, Xiamen, Fujian 361005, China

Rui Zeng - Department of Chemistry and Chemical Biology, Cornell University, Ithaca, New York 14853, United States; orcid.org/0000-0002-7577-767X

Xinran Feng - Department of Chemistry and Chemical Biology, Cornell University, Ithaca, New York 14853, United

Hongsen Wang – Department of Chemistry and Chemical Biology, Cornell University, Ithaca, New York 14853, United States; orcid.org/0000-0001-7926-2895

Weixuan Xu - Department of Chemistry and Chemical Biology, Cornell University, Ithaca, New York 14853, United States

Xinyao Lu – Department of Chemistry and Chemical Biology, Cornell University, Ithaca, New York 14853, United States; orcid.org/0000-0002-2649-5721

Complete contact information is available at: https://pubs.acs.org/10.1021/jacs.2c00518

Author Contributions

§H.L., R.Z., and X.F. contributed equally to this work.

Notes

The authors declare no competing financial interest.

ACKNOWLEDGMENTS

This work was supported as part of the Center for Alkaline Based Energy Solutions (CABES), an Energy Frontier Research Center funded by the U.S. Department of Energy (DOE), Office of Science, Office of Basic Energy Sciences under Grant DE-SC-0019445. This work made use of TEM facilities of the Cornell Center for Materials Research (CCMR), which are supported through the NSF MRSEC (DMR-1719875). This research used resources of the Advanced Photon Source (APS), a U.S. Department of Energy Office of Science User Facility operated for the DOE Office of Science by Argonne National Laboratory under Contract No. DE-AC02-06CH11357. We greatly appreciate the assistance of DND-CAT staff Qing Ma. H.Q.L. is grateful to the China Scholarship Council (CSC) for financial support.

REFERENCES

- (1) Thompson, S. T.; Peterson, D.; Ho, D.; Papageorgopoulos, D. Perspective—The Next Decade of AEMFCs: Near-Term Targets to Accelerate Applied R&D. J. Electrochem. Soc. 2020, 167, No. 084514.
- (2) Lima, F. H. B.; Zhang, J.; Shao, M. H.; Sasaki, K.; Vukmirovic, M. B.; Ticianelli, E. A.; Adzic, R. R. Catalytic Activity—d-Band Center Correlation for the $\rm O_2$ Reduction Reaction on Platinum in Alkaline Solutions. *J. Phys. Chem. C* **2006**, *111*, 404–410.
- (3) Sun, Y.; Zhang, X.; Luo, M.; Chen, X.; Wang, L.; Li, Y.; Li, M.; Qin, Y.; Li, C.; Xu, N.; Lu, G.; Gao, P.; Guo, S. Ultrathin PtPd-Based Nanorings with Abundant Step Atoms Enhance Oxygen Catalysis. *Adv. Mater.* **2018**, *30*, No. 1802136.
- (4) Guo, J.; Gao, L.; Tan, X.; Yuan, Y.; Kim, J.; Wang, Y.; Wang, H.; Zeng, Y.-J.; Choi, S.-I.; Smith, S. C.; Huang, H. Template-Directed Rapid Synthesis of Pd-Based Ultrathin Porous Intermetallic Nanosheets for Efficient Oxygen Reduction. *Angew. Chem., Int. Ed.* **2021**, 60, 10942–10949.
- (5) Yang, Y.; Chen, G.; Zeng, R.; Villarino, A. M.; DiSalvo, F. J.; van Dover, R. B.; Abruña, H. D. Combinatorial Studies of Palladium-Based Oxygen Reduction Electrocatalysts for Alkaline Fuel Cells. *J. Am. Chem. Soc.* **2020**, *142*, 3980–3988.
- (6) Li, C.; Yuan, Q.; Ni, B.; He, T.; Zhang, S.; Long, Y.; Gu, L.; Wang, X. Dendritic Defect-Rich Palladium—Copper—Cobalt Nanoalloys as Robust Multifunctional Non-Platinum Electrocatalysts for Fuel Cells. *Nat. Commun.* **2018**, *9*, 3702.
- (7) Zhou, M.; Guo, J.; Zhao, B.; Li, C.; Zhang, L.; Fang, J. Improvement of Oxygen Reduction Performance in Alkaline Media by Tuning Phase Structure of Pd—Bi Nanocatalysts. *J. Am. Chem. Soc.* **2021**, *143*, 15891–15897.
- (8) Ge, Y.; Wang, X.; Huang, B.; Huang, Z.; Chen, B.; Ling, C.; Liu, J.; Liu, G.; Zhang, J.; Wang, G.; Chen, Y.; Li, L.; Liao, L.; Wang, L.; Yun, Q.; Lai, Z.; Lu, S.; Luo, Q.; Wang, J.; Zheng, Z.; Zhang, H. Seeded Synthesis of Unconventional 2H-Phase Pd Alloy Nanomaterials for Highly Efficient Oxygen Reduction. J. Am. Chem. Soc. 2021, 143, 17292–17299.
- (9) Luo, M.; Zhao, Z.; Zhang, Y.; Sun, Y.; Xing, Y.; Lv, F.; Yang, Y.; Zhang, X.; Hwang, S.; Qin, Y.; Ma, J.-Y.; Lin, F.; Su, D.; Lu, G.; Guo, S. PdMo Bimetallene for Oxygen Reduction Catalysis. *Nature* **2019**, 574, 81–85.
- (10) Wang, L.; Zeng, Z.; Gao, W.; Maxson, T.; Raciti, D.; Giroux, M.; Pan, X.; Wang, C.; Greeley, J. Tunable Intrinsic Strain in Two-Dimensional Transition Metal Electrocatalysts. *Science* **2019**, *363*, 870–874.
- (11) Wang, S.; Tian, D.; Wang, X.; Qin, J.; Tang, Y.; Zhu, J.; Cong, Y.; Liu, H.; Lv, Y.; Qiu, C.; Gao, Z.; Song, Y. Uniform PdH0.33 Nanodendrites with a High Oxygen Reduction Activity Tuned by Lattice H. *Electrochem. Commun.* **2019**, *102*, 67–71.
- (12) Lu, Y.; Wang, J.; Peng, Y.; Fisher, A.; Wang, X. Highly Efficient and Durable Pd Hydride Nanocubes Embedded in 2D Amorphous NiB Nanosheets for Oxygen Reduction Reaction. *Adv. Energy Mater.* **2017**, *7*, No. 1700919.
- (13) Kodama, K.; Nagai, T.; Kuwaki, A.; Jinnouchi, R.; Morimoto, Y. Challenges in Applying Highly Active Pt-Based Nanostructured Catalysts for Oxygen Reduction Reactions to Fuel Cell Vehicles. *Nat. Nanotechnol.* **2021**, *16*, 140–147.
- (14) Fan, J.; Chen, M.; Zhao, Z.; Zhang, Z.; Ye, S.; Xu, S.; Wang, H.; Li, H. Bridging the Gap between Highly Active Oxygen Reduction Reaction Catalysts and Effective Catalyst Layers for Proton Exchange Membrane Fuel Cells. *Nat. Energy* **2021**, *6*, 475–486.
- (15) Li, Q.; Peng, H.; Wang, Y.; Xiao, L.; Lu, J.; Zhuang, L. The Comparability of Pt to Pt-Ru in Catalyzing the Hydrogen Oxidation Reaction for Alkaline Polymer Electrolyte Fuel Cells Operated at 80 °C. Angew. Chem. **2019**, 131, 1456–1460.
- (16) Duan, H.; Yan, N.; Yu, R.; Chang, C.-R.; Zhou, G.; Hu, H.-S.; Rong, H.; Niu, Z.; Mao, J.; Asakura, H.; Tanaka, T.; Dyson, P. J.; Li, J.; Li, Y. Ultrathin rhodium nanosheets. *Nat. Commun.* **2014**, *5*, 3093.

- (17) Zhang, J.; Chen, M.; Li, H.; Li, Y.; Ye, J.; Cao, Z.; Fang, M.; Kuang, Q.; Zheng, J.; Xie, Z. Stable Palladium Hydride as a Superior Anode Electrocatalyst for Direct Formic Acid Fuel Cells. *Nano Energy* **2018**, *44*, 127–134.
- (18) Johnson, N. J. J.; Lam, B.; MacLeod, B. P.; Sherbo, R. S.; Moreno-Gonzalez, M.; Fork, D. K.; Berlinguette, C. P. Facets and Vertices Regulate Hydrogen Uptake and Release in Palladium Nanocrystals. *Nat. Mater.* **2019**, *18*, 454–458.
- (19) Kabiraz, M. K.; Kim, J.; Lee, W.-J.; Ruqia, B.; Kim, H. C.; Lee, S.-U.; Kim, J.-R.; Paek, S.-M.; Hong, J. W.; Choi, S.-I. Ligand Effect of Shape-Controlled β -Palladium Hydride Nanocrystals on Liquid-Fuel Oxidation Reactions. *Chem. Mater.* **2019**, *31*, 5663–5673.
- (20) Bugaev, A. L.; Usoltsev, O. A.; Guda, A. A.; Lomachenko, K. A.; Pankin, I. A.; Rusalev, Y. V.; Emerich, H.; Groppo, E.; Pellegrini, R.; Soldatov, A. V.; van Bokhoven, J. A.; Lamberti, C. Palladium Carbide and Hydride Formation in the Bulk and at the Surface of Palladium Nanoparticles. *J. Phys. Chem. C* 2018, 122, 12029–12037.
- (21) Hoshi, N.; Nakamura, M.; Maki, N.; Yamaguchi, S.; Kitajima, A. Structural Effects on Voltammograms of the Low Index Planes of Palladium and $Pd(S)-[n(1\ 0\ 0)\times(1\ 1\ 1)]$ Surfaces in Alkaline Solution. *J. Electroanal. Chem.* **2008**, 624, 134–138.
- (22) Kiguchi, F.; Nakamura, M.; Hoshi, N. Cation Effects on ORR Activity on Low-Index Planes of Pd in Alkaline Solution. *Electrochemistry* **2021**, *89*, 145–147.
- (23) Ma, X.-Y.; Chen, Y.; Wang, H.; Li, Q.-X.; Lin, W.-F.; Cai, W.-B. Electrocatalytic Oxidation of Ethanol and Ethylene Glycol on Cubic, Octahedral and Rhombic Dodecahedral Palladium Nanocrystals. *Chem. Commun.* **2018**, *54*, 2562–2565.
- (24) Kiguchi, F.; Nakamura, M.; Hoshi, N. Structural Effects on the Activity for the Oxygen Reduction Reaction on the High-Index Planes of Palladium in Alkali Solution. *Electrocatalysis* **2021**, *12*, 691–697.
- (25) Davis, R. E.; Horvath, G. L.; Tobias, C. W. The Solubility and Diffusion Coefficient of Oxygen in Potassium Hydroxide Solutions. *Electrochim. Acta* 1967, 12, 287–297.
- (26) Jiang, L.; Hsu, A.; Chu, D.; Chen, R. Size-Dependent Activity of Palladium Nanoparticles for Oxygen Electroreduction in Alkaline Solutions. *J. Electrochem. Soc.* **2009**, *156*, B643.
- (27) Geniès, L.; Faure, R.; Durand, R. Electrochemical Reduction of Oxygen on Platinum Nanoparticles in Alkaline Media. *Electrochim. Acta* 1998, 44, 1317–1327.
- (28) Khudhayer, W. J.; Kariuki, N. N.; Wang, X.; Myers, D. J.; Shaikh, A. U.; Karabacak, T. Oxygen Reduction Reaction Electrocatalytic Activity of Glancing Angle Deposited Platinum Nanorod Arrays. J. Electrochem. Soc. 2011, 158, B1029.

NOTE ADDED AFTER ASAP PUBLICATION

This paper was published ASAP on April 29, 2022 with a typo in the article title. The corrected version was reposted on May 3, 2022.